Research papers

Bayesian hydrograph separation in a minimally gauged alpine volcanic watershed in central Chile

Katherine H. Markovich[a,d,*,1], Helen E. Dahlke[a], José Luis Arumí[b,d], Reed M. Maxwell[c,d], Graham E. Fogg[a,d]

[a] *Hydrologic Sciences Graduate Group, University of California, Davis, Davis, CA, USA*
[b] *Departmento de Recursos Hídricos, Universidad de Concepción, Chillán, Chile*
[c] *Department of Geology and Geological Engineering, Colorado School of Mines, Golden, CO, USA*
[d] *Climate Change, Water, and Society (CCWAS), Integrative Graduate Research Education and Traineeship (IGERT), Davis, CA, USA*

ARTICLE INFO

ABSTRACT

This study examines the question of how much information one can extract from a tracer-based hydrograph separation in a remote and minimally gaged alpine catchment in Chile. We combine PCA-based endmember mixing analysis to identify the sources of flow contribution to the Diguillín River with a hierarchical Bayesian mixing model to integrate spatial and temporal variability in endmember concentration and quantify the source contributions to streamflow over time. The PCA-analysis shows that precipitation isotopes do not vary by elevation (e.g. snow and rainfall had identical signatures) but vary significantly by season, and that a third endmember is necessary to bound streamflow variability at the basin outlet, which was not captured by our field sampling. One of the main advantages of Bayesian methods is the quasi-machine learning capabilities, where we treated the third endmember as a parameter from which the mixing model could both estimate proportional contributions as well as posterior estimates for the tracer concentrations.

The two tracer, three endmember hydrograph separation revealed groundwater to be the largest and precipitation (rain and snow) to be the smallest contributor, on average, to streamflow with the third unknown endmember contributing around 40% of streamflow during the Winter wet season. We hypothesize that interflow is occurring as the third endmember in the Alto Diguillín subwatershed, based on inferred tracer values and the presence of alluvium atop impermeable bedrock along certain reaches. More work is necessary to observe and sample these flowpaths, which was not possible during this study. The results of this work have implications for water resource management, since groundwater sustains the majority of streamflow in the Diguillín, and climate change will impact the timing and quantity of baseflow and interflow. Overall, we demonstrate the utility of combining PCA with Bayesian statistical modeling and inference to extract maximum information from a limited field dataset in a remote alpine catchment. The findings of this work can guide future water management in the Diguillín, but also provide clear questions for future research.

1. Introduction

Snowmelt-dominated and snowmelt-dependent regions are highly susceptible to climate change due to the warming effect on snow, glaciers, and ecosystems (Barnett et al., 2005; Beniston et al., 1997; Cristea et al., 2014; Mankin et al., 2018). While detection and attribution at the regional (i.e. watershed) scale remains challenging, there is strong consensus that snowpack and vegetation shifts will alter mountain water supply in response to climate change. Precipitation phase is shifting from snow to rain (Knowles et al., 2006), and the snowpack is melting sooner (Barnett et al., 2005; Musselman et al., 2017), shifting the historical timing of water supply (Ficklin et al., 2013; Hidalgo et al., 2009). Migrating tree lines, increased net primary production, and shorter dormant seasons (Cristea et al., 2014; Goulden and Bales, 2014) are leading to increased winter evapotranspiration (ET) in alpine settings, though the extent to which this is offset by decreased ET in the increasingly dry summer seasons is uncertain. A major challenge in understanding these shifts in water supply and availability in alpine regions is the general lack of monitoring data.

One way that hydrologists have approached this challenge in

---

characterizing alpine water budgets is through the use of environmental tracers. These passive and ubiquitous tracers are relatively affordable and simple to collect, and can provide information on sources and mixing of sources in a watershed. These sources can be quantified via hydrograph separation (HS), provided they are sufficiently known or characterized, that they mix conservatively, and that they are distinguishable from other sources (Buttle, 1994; Klaus and McDonnell, 2013; Sklash et al., 1976). If these assumptions are met, the sources form a linear combination of *n* components using *n* − 1 tracers and can be separated using a simple mass balance:

$$Q_T c_T = Q_1 c_1 + Q_2 c_2 + \cdots + Q_n c_n \tag{1}$$

where Q_T is total streamflow (volume/time), Q_1, Q_2, ...Q_n are the source components to runoff, and c is the observed concentration of streamflow and components. Studies have used this HS method to quantify sources of snow (Taylor et al., 2001; Taylor et al., 2002), glacier melt (Cable et al., 2011; Dahlke et al., 2014; Rodriguez et al., 2016), soil water (Christophersen and Hooper, 1992), and groundwater (Muñoz-Villers and McDonnell, 2012) to streamflow in alpine systems. As the novelty of HS has settled (Burns, 2002), hydrologists now focus their efforts on reducing uncertainty in this method.

In this new phase of HS, several questions merit attention. First, how well does one know the endmembers contributing to streamflow at any point in time (Christophersen and Hooper, 1992; Liu et al., 2008)? Early HS studies developed a two endmember conceptual model of *pre-event* water, or any water in the stream or subsurface prior to the event, and *event* water, or any rain or snow that contributes to streamflow from the event (Buttle, 1994). As HS methods matured, hydrologists have been able to parse out multiple endmembers such as snow versus rain in the event category and groundwater versus soil water in the pre-event contributions, which better inform our understanding of runoff-generation processes in catchments (Klaus and McDonnell, 2013). It remains a challenge, however, to determine the "true" endmembers contributing to streamflow based on the streamflow mixture, since we often have imperfect knowledge of the runoff generating processes occurring, especially in remote, alpine basins.

Principal component analysis (PCA) is a useful tool for decomposing streamwater chemistry with the goal of identifying the number of sources in the mixture (Christophersen and Hooper, 1992). In its essence, PCA takes centered (subtracting the mean) data and uses the correlation matrix to reduce the dimensionality of the dataset, where the first and second axes can often explain >90% of the variation contained within streamwater chemistry. The main advantage to using PCA for hydrograph separation is the ability to identify the number of endmembers to use in the mixing model, which greatly reduces conceptual uncertainty. Hooper (2003) presented a methodology for the unambiguous identification of endmembers, and Liu et al. (2008) developed a method for further evaluating the eligibility of endmembers. These methods have formed the basis for applications of endmember mixing analysis (EMMA) in a range geoclimatic settings (Bearup et al., 2014; Rodriguez et al., 2016; Zhang et al., 2018).

Secondly, given that we know the endmembers, how can we appropriately measure and characterize their spatial (Fischer et al., 2017; Ogle et al., 2014; Ohlanders et al., 2013) and temporal (Klaus and McDonnell, 2013; Mcintosh et al., 1999; Schmieder et al., 2016) variability in our hydrograph separation? For example, studies have shown that rain isotopes can vary significantly within and between events (McDonnell et al., 1990), and snowpack evolution can produce distinct melt signatures throughout a season (Taylor et al., 2001; Taylor et al., 2002). Much of this variability can be captured by thorough and strategic sampling design. However, incorporating seasonally and spatially-varying endmember concentrations remains a challenge in traditional linear HS models. Finally, the traditional hydrograph separation model assumes streamflow is a linear combination of *n* endmembers (Eq. (1)), and this approach relies on ad hoc uncertainty analysis and error propagation (Genereux, 1998). Such an approach can be quite reliable in highly instrumented alpine watersheds with spatially and temporally extensive chemistry data, such as experimental forests and watersheds, however the potential for uncertainty in remote and minimally-gauged watersheds is much greater.

Bayesian methods are well suited for the problem of source variability and parameter estimation, since they incorporate prior knowledge along with observations. Furthermore, through the use of Monte Carlo Markov Chains (MCMC) one can efficiently handle the computational burden of solving for large numbers of parameters. Simple linear mixing models can be implemented in a Bayesian framework, which has the advantage of automatically incorporating analytical, spatiotemporal, and random uncertainty and propagating the combined uncertainties throughout the analysis (Arendt et al., 2015). Recent Bayesian hydrograph separation studies have gone beyond simple linear mixing models to add nonlinear effects accounting for processes occurring in the watershed, such as spatial or temporal autocorrelation (Ogle et al., 2014). In particular, Cable et al. (2011) was able to estimate proportions of glacial contribution to streamflow in the remote Wind River range of Wyoming by adding a hierarchical distance decay function, meaning glacier contributions automatically decrease with increasing distance in their mixing model. They showed how the hierarchical Bayesian mixing model significantly reduced uncertainty in the posterior estimates of source contribution when compared to the simple linear mixing model (Cable et al., 2011). Mailloux et al. (2014) demonstrated the utility of incorporating prior information in Bayesian hydrograph separation by developing a hierarchical Bayesian mixing model to estimate contributions from specific geologic formations along a longitudinal survey. While Bayesian methods are clearly powerful for incorporating and reducing parameter uncertainty, they rely on conceptual knowledge to construct the mixing model. Ultimately, the strengths of a PCA-based endmember identification with that of a hierarchical Bayesian mixing model are highly complementary and ideally suited for hydrograph separation in data poor catchments.

Here we present the application of a hierarchical Bayesian mixing model in a remote and minimally-gauged alpine watershed in central Chile to answer two questions: (1) What are the dominant sources contributing to streamflow in the Diguillín watershed? and (2) How do these sources vary across seasons? We discuss the utility in merging these techniques to reduce parameter and ultimately conceptual model uncertainty as well as to identify areas for future work, given a limited dataset. We conclude with water resource implications of this analysis for the Diguillín watershed with respect to climate change.

2. Study area and methods

2.1. Site background

Located in the Andes Cordillera of Central Chile, the Diguillín Watershed has a Mediterranean climate with cool, wet winters, and warm, dry summers. Average temperature is 12.4 °C, and ranges from 6 °C in winter to 20 °C in summer, and average precipitation is 1750, 415, and 115 mm for winter, spring, and summer, respectively (Arumí et al., 2012). Uplands and headwaters of the watershed receive significant amounts of snow, but much of the catchment is sufficiently low in elevation (e.g. 50% is below 2000 masl) to be rain-dominated year-round, resulting in hydrographs that typically peak in winter due to rain, followed by smaller snowmelt peaks in spring (Fig. 1).

The catchment drains 334 km², including the Nevados de Chillan volcanic complex, and contains two subwatersheds: the Renegado (127 km²) and the Alto Diguillín (207 km²) (Fig. 2). Land use differs dramatically in the two subwatersheds. Much of the Alto Diguillín is a National Forest Reserve and is thus sparsely populated, while the Renegado contains a growing tourism and vacation home industry associated with the Nevados de Chillan ski resort. Land cover is largely deciduous forest, with some conifer species in the Nuble Reserve in the Alto Diguillín, and the lower portions of the Alto Diguillín
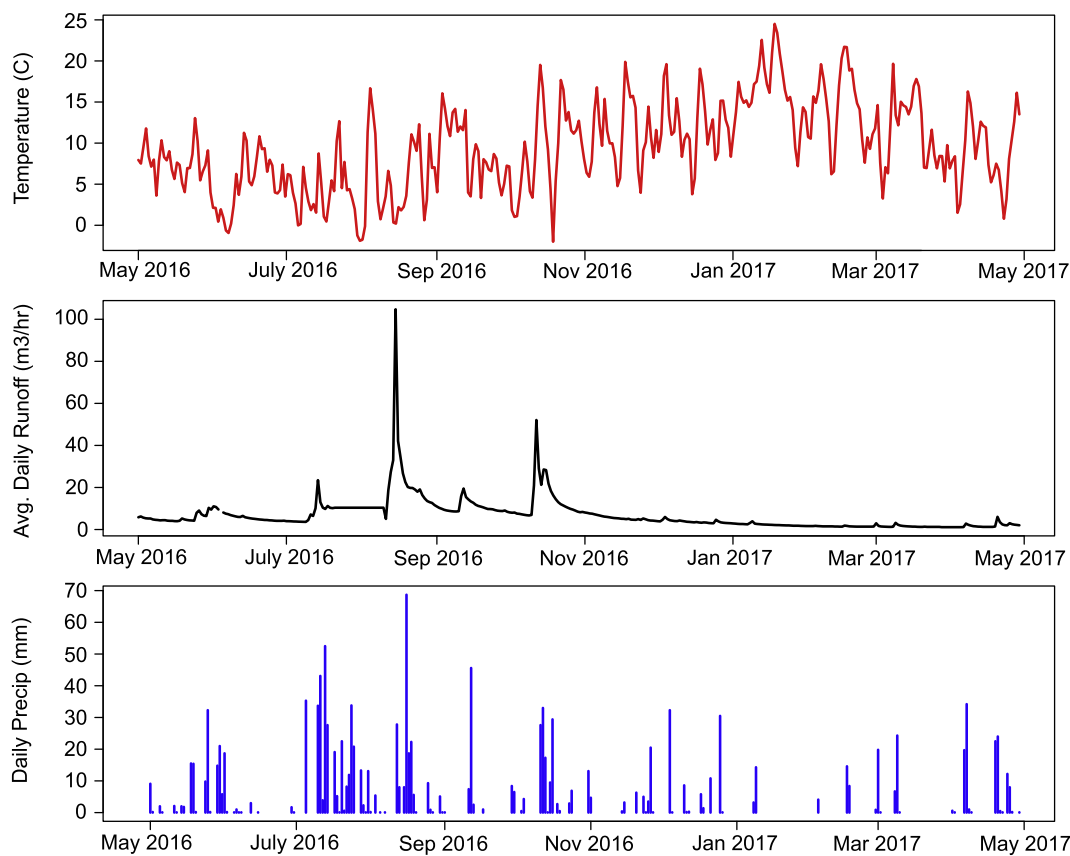
Fig. 1. Time series of temperature, average daily discharge, and cumulative daily precipitation from the Diguillín San Lorenzo station.

subwatershed contain forest plantations of pine and eucalyptus as well as agricultural land.

These basins are hydrogeologically distinct yet connected. Importantly, the Renegado is perched topographically higher than the Alto Diguillín by up to 1000 m in the upper portion of the

subwatersheds. This creates significant potential for interbasin groundwater flow from the former to the latter (Frisbee et al., 2016). The Alto Diguillín basin is predominantly comprised of the Cura-Malin formation, a mix of conglomerates, breccias, sandstones, clays, tuffs, with intercalations of limestone and andesitic-dasitic lavas, and is
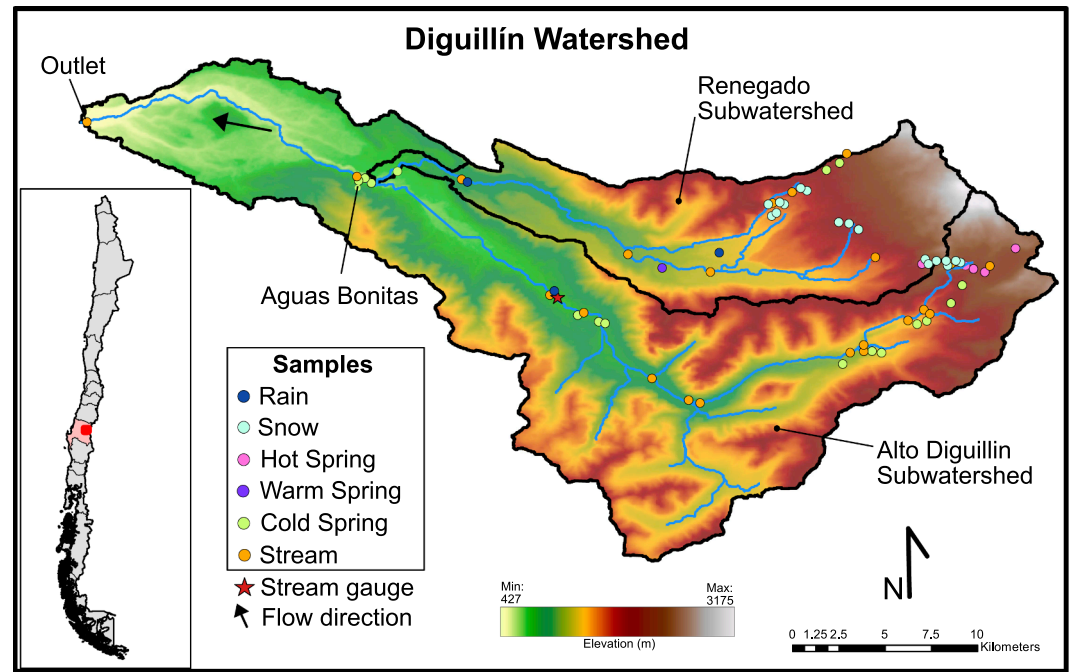

Fig. 2. Map of the Diguillín Watershed, with the sampling points, gaging station, two subwatersheds, and high volume spring complex (Aguas Bonitas) labeled. Flow is from east to west, indicated by the arrow.

estimated to be in the range of Cretaceous to Eocone-Oligocene (Dixon et al., 1999). This low formation comprises the glacially-eroded uplands of the Alto Diguillín subwatershed, while alluvial and colluvial deposits derived from the Cura-Malin formation comprise the valley fill. The headwaters of the Diguillín emanate from a series of high-volume, thermal springs in a high alpine valley adjacent to the north end of the Nevados de Chillín volcanic complex. This valley, aptly named Valle de Aguas Calientes (Valley of Hot Waters), is filled with volcanic flow, ash, and lahar deposits owing to its proximity to the active volcanic centers. Hot spring fed streams as well as snowmelt-fed streams feed into the Diguillín in this valley before it reaches the valley terminus, drops down 700 meters, and continues flowing westward to the Pacific Ocean (Fig. 2).

The Renegado subbasin, like Valle de Aguas Calientes, exhibits a recent and explosive geologic history, with massive sub-glacial ande-sitic-dasitic flows, and pyroclastic deposits lining the valley walls, and more recent post-glacial flows exposed in the upper portion of the valley (Dixon et al., 1999). The valley floor of the Renegado consists of Holocene lahar deposits, exposed through river cuts. Soils are similarly comprised of sandy volcanic ash, with very high infiltration capacities evidenced by the rare occurrence of ponded water. Outcropping be-tween the two subwatersheds is the massive Santa Gertrudis felsic ig-neous batholith. The hydrologic connection between these two catch-ments occurs both in the surface and the subsurface. The Renegado stream flows West until it hits a lower permeability volcanic deposit and turns dramatically south to flow into the Diguillín River (Fig. 2). Interestingly, the Renegado stream often 'disappears' right before this turn, and then reappears downstream in the form of a high volume spring. Additionally, Arumí et al. (2012) found a series of high volume springs just downstream of this surface connection, which from a simple mass balance estimate, seem to account for the "missing" water in the Renegado water budget. Preliminary particle tracking results showed that these springs could indeed be fed by groundwater in the Renegado basin (Arce, 2014), but questions remain as to how much water and what flowpaths feed these springs, which sustain flow in the Diguillín river through the dry season. Furthermore, it is unclear what proportion of water is fed from snow, rain, and groundwater in the Diguillín above the Renegado junction. These unknowns motivate the use of environ-mental tracers to better understand the surface, subsurface, and inter-basin flowpaths in the Diguillín watershed, the methods of which we describe below.

2.2. Field and laboratory analysis

We collected water and snow samples at different locations in the Diguillín watershed across three field campaigns during 2016–17: a winter campaign from June to August, a spring campaign in October, and a late summer campaign from February to April. Funding and travel limited our ability to collect samples on a continuous weekly basis throughout the year, however we designed the fieldwork trips to cover the major seasonal variation in sources. We hypothesized the sources to be snow, rain, and groundwater, and therefore we collected samples of these sources across the three seasonal field campaigns with as much spatial coverage as possible (Fig. 2). Road closures, however, limited access to much of the Alto Diguillín watershed in the winter and spring seasons. Snow samples were collected during both the winter and spring campaigns, by digging pits and sampling every 10 cm for tem-perature and density, and also using a Kovacs Coring System ice drilling core for depth-integrated samples. Snow samples were tightly bagged and kept frozen in the field, and then slowly melted in a fridge to prevent fractionation. The snow samples were grouped by geographic location, weighted by the estimated snow water equivalent, and then the median value for each pit was used in analysis. This was done to capture values for snow that were not disproportionately influenced by sublimation near the surface or melt and redistribution near the base. In total, 10 snow pits were dug and 10 cores were collected, representing

the dominant snow contributing areas and covering a range of aspect and elevation (1400–2400 masl).

Throughout each of the field campaigns, weekly samples of streamflow in the Alto Diguillín, Renegado, and Diguillín watershed outlet were taken. All water samples were collected in 15 ml centrifuge bottles, with minimal headspace to prevent evaporation. Field mea-surements of electrical conductivity (EC) and pH were taken concurrent with each sample. These samples were refrigerated until analysis. In absence of accessible wells in the Diguillín watershed, samples of spring water in both subwatersheds were collected seasonally in order to characterize the groundwater source. Rain samples were collected by installing a funnel in an area clear of vegetation attached by plastic tubing to a 1 liter Nalgene bottle containing mineral oil to prevent evaporation. The rain samples were difficult to collect owing to a lack of access to areas where sampling equipment would be protected, and thus only 10 samples of rain where collected throughout the sampling seasons.

Samples were analyzed for stable isotopes Deuterium (δD) and Oxygen-18 ($\delta^{18}O$) at the UC Davis Stable Isotope Facility using a Laser Water Isotope Analyzer V2 (Los Gatos Research, Inc., Mountain View, CA, USA). Each sample is injected at least six times, and the average of the last four injections is used for isotope ratio calculations. Sample isotope ratios are standardized using reference water, which was cali-brated against Vienna Standard Mean Ocean Water (VSMOW). Precision for water samples at natural abundance is typically $\leqslant 0.3‰$ for $\delta^{18}O$ and $\leqslant 2.0‰$ for δD. Final $\delta^{18}O$ and δD values are reported re-lative to VSMOW. The samples were also analyzed for *Ca*, *Mg*, *Na*, *K*, *Fe*, *Sr*, *Cl*, and *Si* at the UC Davis Interdisciplinary Center for Plasma Mass Spectrometry on a triple quadropole ICPMS (Agilent 8900 ICPMS). Abundances were measured using H^2 or He collision cell gas in MSMS mode and are herein reported as con-centrations (mg/L).

Water samples for cations and anions were analyzed from remaining water samples after isotope analysis, and thus were not filtered or preserved. Although not ideal, because our aim was to distinguish be-tween endmembers rather than to quantify concentrations for geo-chemical analysis, we believe the data are adequate for our mixing model purposes. All samples were kept refrigerated and exposed to the same sampling method and waiting times. As an added check, we compared our data to unpublished data from a previous sampling campaign (2011–13) that field filtered and preserved their samples for water chemistry for several overlapping sites. Our laboratory results for anions and cations agreed with the results from the 2011–13 sampling campaign. This suggests that abiotic or biogeochemical processes within the sampling bottles did not significantly influence the dissolved concentrations of the anions and cations we considered.

2.3. Principal component analysis

We first screened the solute data to identify conservative tracers suitable for principal component analysis (PCA) using bivariate re-gressions with criteria suggested by Hooper (2003) of collinear struc-ture and an r^2 value > 0.5 ($p < 0.05$). From this we eliminated K from the set of conservative tracers and performed a PCA using the R package *factoextra* (Kassambara, 2017) on the normalized and centered stream (mixture) and endmember (source) samples. From this, we can identify *n*, the rank of the mixture (e.g. the number of axes). Since we are using mean-centered data, the number of endmembers must equal $n + 1$. The methods outlined by Hooper (2003) are useful if there is only mixture data available, and one assumes that endmembers bound the mixture data in lower dimensional space. A possible disadvantage to this ap-proach is that it is difficult to inversely determine the provenance of streamflow, due to non-unique mixing processes and catchment het-erogeneity. Hence, we decided to use a forward approach by sampling all possible sources, including rain, snow, thermal and meteoric groundwater and PCA to ascertain endmembers and the most
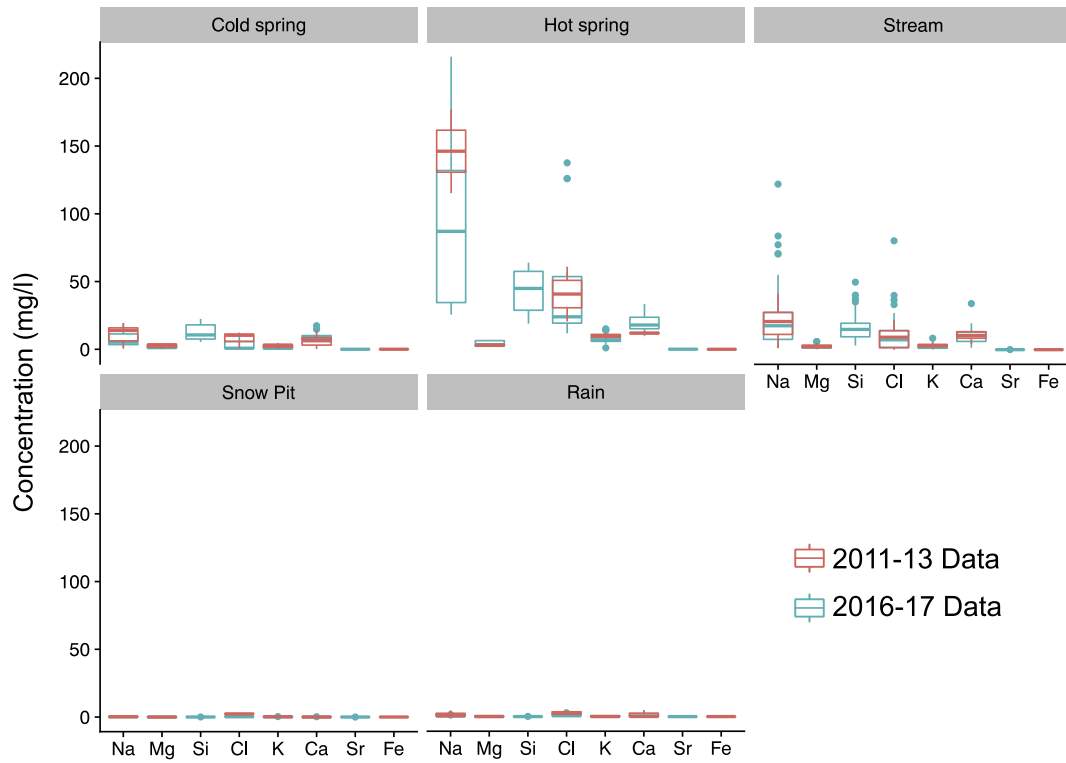
Fig. 3. Box and whisker plots of water chemistry data, colored by sampling campaign. The upper and lower box limit represents the first and third quartile of sample concentrations, the line represents the median, the whiskers encompass the maximum and minimum, and points represent outliers.

explanatory solutes (Zhang et al., 2018). The resultant number of endmembers and tracer concentrations are then implemented in a hierarchical Bayesian mixing model to perform the hydrograph separation for quantifying source contributions.

2.4. Bayesian mixing model

We implemented the mixing model in R using *rstan* (Stan Development Team, 2018). Stan is a Bayesian modeling and inference tool that employs a Hamiltonian MCMC primarily using the No-U Turn (NUTS) sampler (Hoffman and Gelman, 2014). At its core, we implement a linear mixing model akin to Eq. (1), however we add a varying effect for time in order to estimate the seasonal variability of source contributions. The resultant master equation of n endmembers and i observations is:

$$[\mu_{\text{stream}}]_{[i]} = \sum_{j=1}^{n} (p_{j[i]} + p.\,week_{j[i]}) \cdot C_{j[i]} \tag{2}$$

where μ_{stream} is the mean tracer value for the linear combination of endmember mean concentration values (C) multiplied by their proportional contribution (p) plus a varying effect for time ($p.\,week$). This varying effect treats the weekly samples as independent, which is reasonable given the coarse temporal resolution. The endmember proportions are constrained to 1 for each modeled time-step using the softmax function,

$$a_{[j]} = \frac{exp(p_{[j]} + p.\,week_{[j]})}{\sum\limits_{k=1}^{K} exp(p_{[k]} + p.\,week_{[k]})} \, for j = 1...K \tag{3}$$

$$\sum_{K} a_{[j]} = 1 \tag{4}$$

where $p + p.\,week$ is the time-varying proportion of endmember j, k is the transformed logit, K is the total number of endmembers, and a is the

softmax. This procedure allows for hydrograph separation without knowing streamflow discharge at the outlet, making it highly useful for ungauged basins. We assign weak normal priors for the varying intercept parameters ($p.\,week$) and standard normal priors on the process model parameters (p). The variance for both is modeled with a weak exponential prior with expected value of 1. We checked all sampling data for normality via Q-Q plots, and found the assumption to be unreasonable given the thick-tailed distribution of our data. Thus we assign a student-t distribution likelihood with mean equal to μ_{outlet} in Eq. (2), variance equal to an exponential distribution with expected value of 1, and 20 degrees of freedom. This allowed for the Bayesian model to fully explore the tails of the distribution, and significantly improved model fit between observed and predicted values. The number of mixing equations is equal to the number of tracers and time-varying source contributions are constrained to satisfy all mixing equations in the model. The data in this model, for which the hydrograph separation is performed, is a vector ($n = 22$) of the weekly observed concentrations of tracers for the Diguillín outlet (Fig. 2). The observed tracer concentrations are incorporated in the model as the mean and standard deviation from a normal distribution for each endmember. The ability to incorporate endmember tracer concentrations as a distribution allows the model to explore a larger range of possible of values given spatial and temporal variability that we were able to capture in our sampling, thus incorporating uncertainty throughout the process. We then ran the model using four MCMC chains with a warm-up of 1000 iteration steps followed by 1000 simulation steps, resulting in 4000 samples from which we calculated posterior distributions.

3. Results

3.1. Chemistry data

The chemistry results indicate consistent behavior within the types of samples, where the hot spring samples exhibit the highest dissolved concentrations, particularly with *Na*, and the precipitation samples
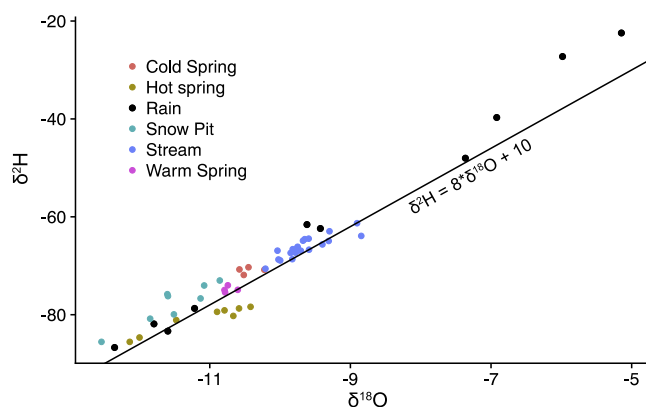
Fig. 4. Stable isotope regression, showing the global meteoric water line (GMWL), and the samples labeled by type.

Fig. 5. Time-series of δD values for thermal springs, cold springs, snow pits, rain, and streamflow samples.

(snow and rain) the lowest (Fig. 3, Table 1). Further, a comparison of the 2016–17 chemistry results with those of the 2011–13 sampling campaign indicates that water chemistry is relatively consistent for the sampled types of water (snow, rain, groundwater, streamflow) between years. This occurs despite inter-annual variability in precipitation, where the period of 2011–13 was wetter by roughly 300 mm of annual precipitation than 2016–17 (Reportes Hidrometeorol, 2018). One noticeable difference between our sampling campaign and the previous is that the hot spring solute concentration exhibits less variability, shown by the smaller range of the first and third quartile, especially for the *Na* concentration, in Fig. 3. We attribute this difference to sampling bias. We collected samples (n = 8) from thermal springs over a broader spatial and temperature range (15–45 °C), whereas the previous sampling campaign collected 2 samples from the same spring in Valle de Aguas Calientes.

3.2. Isotope data

Stable isotope results plot very near the Global Meteoric Water Line (Fig. 4, Table 1). The data does not indicate an altitude effect in precipitation isotopes– rain samples collected following winter storms exhibited isotopic signatures close to that of snow. A study from a glaciated alpine catchment near Santiago found snow to be significantly more depleted than rain, with $\delta^{18}O$ values of $-16‰$ and $-10‰$, respectively (Ohlanders et al., 2013). We propose two hypotheses for why we did not see a significant difference between isotopic values of winter rain and snow samples. First, our snow sampling method prevented giving depleted isotopic values undue weight. Sublimation, melt, and vapor redistribution cause snowpack isotopes to vary considerably with depth. We addressed this uncertainty by sampling isotopes and measuring snow water equivalent (SWE) at 10 cm depth intervals, and then taking the median of the SWE-weighted depth values for each pit. Second, storm source may have more strongly controlled isotopic values for precipitation than altitude in our study. A recent review of stable water isotopic variation in Chile found a clear latitudinal effect between the moisture source of winter and summer precipitation where winter storms contribute depleted isotopes sourced from higher latitude ocean regions (Sanchez-Murillo et al., 2018). Finally, higher frequency (e.g. within storm) and greater spatial coverage of rain samples would better allow for detection of an altitude effect, and so future work should address this question in the Diguillín watershed.

Rain isotopes show wide temporal variation and no clear spatial pattern, consistent with rain isotopic data in other headwaters catchments (Fischer et al., 2017; Knowles et al., 2006; McDonnell et al., 1990). In contrast to the stream and groundwater samples, which are relatively constant throughout the year (Fig. 5), the rain isotopes vary seasonally. In winter, rain isotopes cluster near the snow pit concentrations and then enrich throughout the spring and summer (Fig. 5,
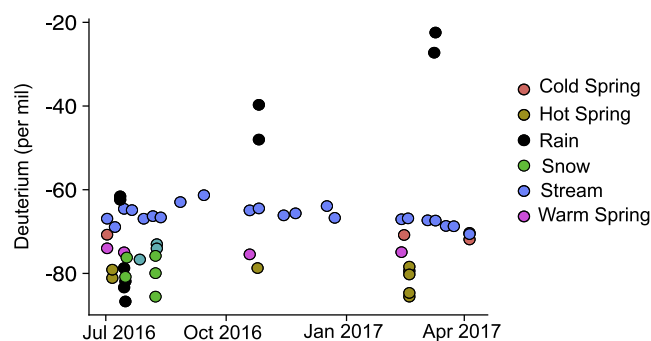
black dots) (Dahlke et al., 2014; Taylor et al., 2001). The timing of when rain samples most resemble snow is key for this Mediterranean catchment, since the majority of precipitation falls during the winter months. The water year 2016–17 was abnormally dry, and so the bulk of precipitation in the Diguillín fell during 4 storm events, 3 of which were captured by this study (Fig. 1). The inability to isotopically distinguish rain from snow during those key storm events motivated this work to explore endmember scenarios alternative to our initial hypothesized three-component (rain, snow, and groundwater) hydrograph separation.

3.3. Principal component analysis

Principal component analysis reduces the dimensionality of data based on inherent correlations in the dataset and assists in identifying the dominant endmembers contributing to streamflow in the Diguillín. The variation in our dataset was reduced from 10 dimensions representing each chemical and isotopic constituent to two dimensions representing solutes and isotopes, respectively (U1 and U2 in Fig. 6). This result further supports the earlier findings that water sources vary consistently based on chemical concentration and isotopic signature, and yet reveals that the underlying processes governing variation in solute concentration and isotopes are distinct. Fig. 6 shows the results of two PCA analyses– the PCA on the left includes hot springs while the PCA on the right excludes hot springs. In both plots, individual observations are plotted with their shape and color determined by the type of sample. The ellipses represent the direction and magnitude of variation for each water source type, and the bold shape represents the ellipse centroid. The combined percentages of PCA axes reflect how well the two axes explain variation in the data points, and the distance between points can be interpreted as a measure of dissimilarity.

In both plots, the horizontal U1 axis, which represents solute concentrations of the water samples, explains the most variation (Fig. 6). The water types spread out horizontally along this axis, with hot springs and precipitation being the most dissimilar. The vertical U2 axis, which represents stable isotope values, explains a smaller fraction of variation, and the precipitation samples separate out most notably along this axis. Depleted winter precipitation samples plot higher along the U2 axis while the enriched summer rain samples plot in the bottom right quadrant.

3.4. Endmember identification

The purpose of using PCA in this study is to identify the major sources of water contributing to streamflow in the Diguillín (Christophersen and Hooper, 1992) for use in the Bayesian hydrograph separation model. The criteria for source selection is that they encapsulate the cloud of streamflow points, essentially bounding the total mixture variation in solute and isotope concentration of the Diguillín river. The distance between the hot spring and the streamflow samples
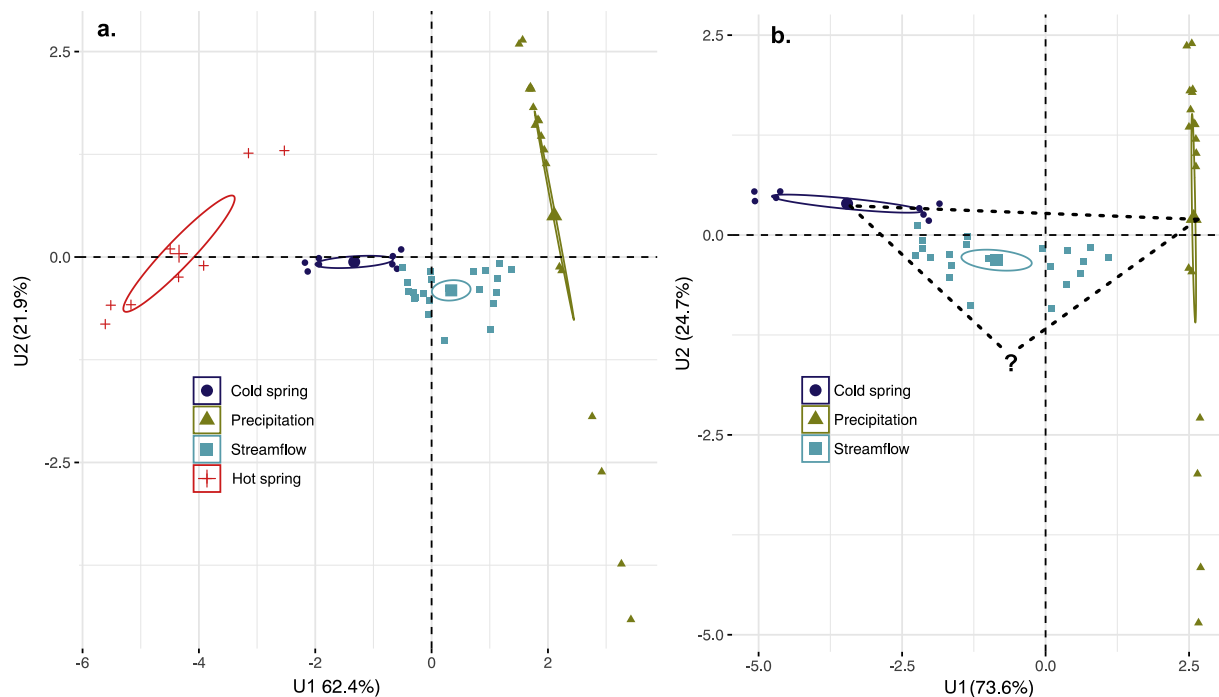
Fig. 6. 2016–17 PCA results for solutes (U1) and stable isotopes (U2) with hot springs included (a.) and excluded (b.). The black dashed triangle in b. represents the mixing space between groundwater, precipitation (rain and snow), and the unknown third endmember.

suggest that the hot spring solute concentrations do not play an important role in the variability of Diguillín streamflow. Samples collected from a longitudinal survey of the Diguillín in March 2017 further confirm this, where the high-solute and depleted-isotope signature of hot springs rapidly diminishes downstream from Valle de Aquas Calientes. From this, we conclude that hot springs are not a major source contributing to streamflow in the Diguillín.

The ellipse centroids for the groundwater and precipitation samples closely bound the upper two corners of the streamflow data cloud (Fig. 6b, dashed line), suggesting that they are major source contributors. It is clear from this plot, however, that a third endmember is required to encompass the full variability of streamflow data (Fig. 6b). While the lower outlying precipitation points could explain some of the streamflow variation along the vertical U2 axis, the distance along the horizontal U1 axis between precipitation and streamflow points suggests that the precipitation endmember alone does not explain the streamflow variation. Thus, we elect to include the third endmember as an unknown source along with the groundwater and precipitation sources in the hierarchical Bayesian mixing model. We explore possible explanations for this unobserved source in Section 4.

3.5. Bayesian hydrograph separation

Here we describe the input and results from our two tracer, three endmember mixing model. We use Si and δD as the two tracers, since the PCA analysis identified these variables as contributing the highest explanatory power for the U1 and U2 axis, respectively. Since solutes and isotopes strongly covary along the U1 and U2 axis, respectively, the tracer choice representing each axis has little impact on the resultant hydrograph separation. The groundwater and precipitation concentrations were assigned informative normal prior distributions, with mean and standard deviation determined from the raw data. The third unknown endmember is assigned weakly informative normal priors, with mean values based on the estimated lower point of the bounding triangle from a $\delta D - Si$ biplot of stream mixture data and a large standard deviation. Given that the prior for this parameter is weakly informative, this estimate for the mean is quickly overcome by the likelihood and

data in the Bayesian model. Thus, we merely give the model a starting point for this third endmember, and allow Bayesian inference to estimate the proportional contribution of this unknown source as well as posterior tracer values for δD and Si.

The hierarchical Bayesian mixing model performed well, as shown by the least squares regression between observed tracer values and the expected value of the posterior distribution for the 22 streamflow outlet samples (Fig. 7). The vertical bars represent 95% confidence intervals around each of the model estimated tracer value drawn from the 4000 samples performed using four Monte Carlo Markov Chains. This allows for the Bayesian model to explore the full joint distribution space of all parameters in the model, given the observed tracer concentrations. The δD tracer estimates showed the best agreement between observed and posterior values, with a regression slope close to one and randomly-distributed residuals. The Si concentrations showed slightly less but still good agreement. The residuals in the Si plot show that the model slightly over predicts Si concentration in the winter months and slightly under predicts Si concentrations in summer months, with a slope of .88 and R^2 of .98 (Fig. 7). Future work could explore increasing the degrees of freedom for the student t-distribution likelihood for the Si tracer, however we deemed these model fits to be more than sufficient. Overall, the dominant seasonal shifts in concentration were reasonably captured across sampling events.

Probability density functions of the posterior distributions of annual proportional contributions from the three modeled endmembers are shown in Fig. 8. Similar to Fig. 7, the expected values and confidence intervals of the posterior distribution for p (Eq. (2)) are calculated from the 4000 simulations of each sampling event. The mean source contributions in water year 2016–17 are 13%, 31%, and 56% for the precipitation, unknown, and groundwater endmember, respectively (Fig. 8). The p estimates are calculated by holding the varying time intercept ($p. week$) constant, and so the uncertainty shown in Fig. 8 is solely related to the uncertainty in endmember concentration. In general, a longer and/or higher frequency dataset would significantly reduce uncertainty in these posterior estimates, particularly for the unknown endmember for which there were no direct measurements of concentration. Overall, the uncertainties contained in the estimated
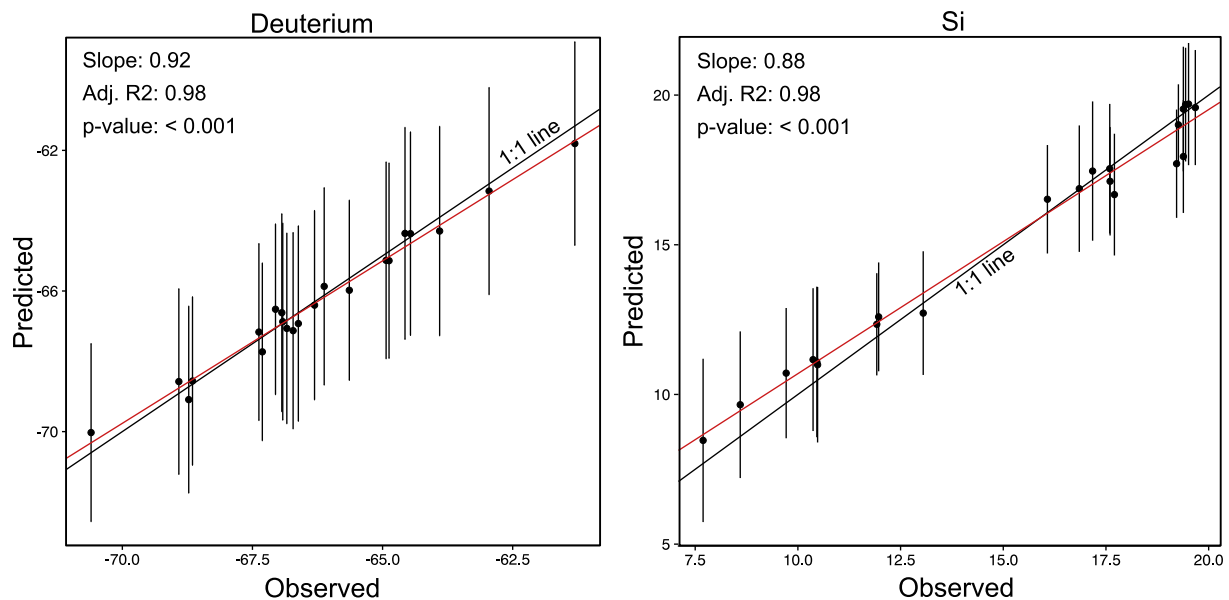
Fig. 7. Least squares regression (red line) of observed tracer concentrations versus the expected value (black points) and 95% confidence interval (vertical black lines) of the posterior distributions of modeled tracers values for δD and Si. Model diagnostic values are given in the upper left hand corners, and a 1:1 line is plotted (in black).
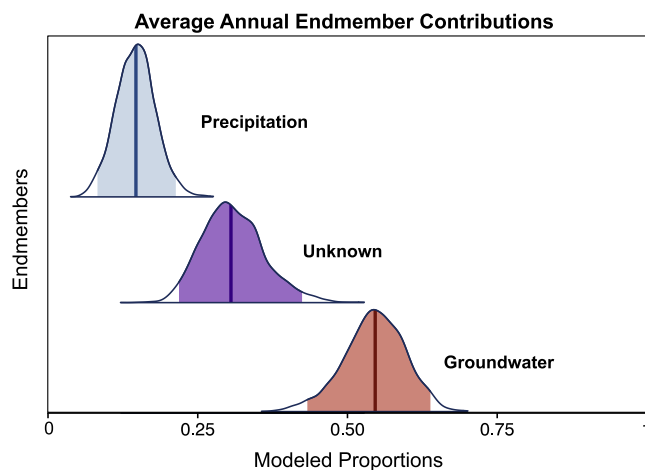
Fig. 8. Probability density functions of the posterior proportional contributions to streamflow for precipitation (blue), unknown (purple), and groundwater (red) endmembers from the two-tracer model. 95% confidence intervals are shown in the shaded regions under the curve.

average annual proportions represent reasonable first approximations given the limited dataset.

The posterior estimates of the time-varying source contributions ($p + p. week$ in Eq. (2)) show a clear seasonality in endmember source contributions (Fig. 9). In this plot, the lines represent posterior averages of source contributions, with error bars representing the 95% confidence intervals of the posterior distribution for each modeled sampling point. Fig. 9 indicates that groundwater contributes as low as 25% of streamflow in the winter wet season and up to 75% of streamflow in the dry summer and fall months of December through April. Not surprisingly, the precipitation source also exhibits seasonality, with most contributions occurring in the wet winter months. The third unknown endmember contributes around 40% of streamflow during the winter season, potentially becoming a larger source proportion than groundwater, though overlapping uncertainty for these two sources during the winter season prevents a conclusive determination of the most dominant contributor. Following the wet season, this unknown endmember decreases steadily, with occasional peaks corresponding with low intensity precipitation events (Fig. 1) from December through April (Fig. 9).

4. Discussion

The main results of this hydrograph separation are that groundwater contributes the majority of streamflow on average, precipitation contributes the least to streamflow, and that a significant proportion of runoff-generation in the Diguillín comes from an unknown third source during the wet season. Here we explore limitations and possible interpretations of these results.
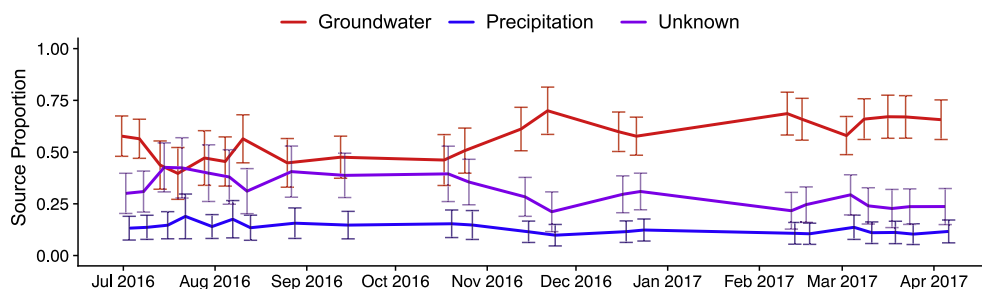
Fig. 9. Hydrograph separation results for water year 2016–17 for precipitation (blue), unknown (purple), and groundwater (red) source proportions. The error bars represent the 95% confidence interval of posterior parameter values based on the MCMC simulations.

4.1. Groundwater

Previous work in the Diguillín watershed has suggested that groundwater is an important source of water to streamflow, based on the discovery of high volume spring complexes and estimation of interbasin losses from the Renegado to the Alto Diguillín subwatersheds (Arumí et al., 2012). Our results support this hypothesis and advance our understanding by quantifying the seasonal proportional contributions of groundwater, relative to other sources. While deep groundwater flowpaths are known to occur in mountain systems regardless of geologic setting (Andermann et al., 2012; Frisbee et al., 2011; Tague and Grant, 2009; Wilson, 2004), it is generally difficult to quantify this source of streamflow owing to a lack of groundwater monitoring data in the mountains. Our study indicates that groundwater contributes roughly 50 − 75% of streamflow depending on the season (Fig. 9), largely from the more permeable Renegado subwatershed "losing" water via springs to the Diguillín. Muñoz-Villers and McDonnell (2012) found similar behavior in an alpine volcanic setting, where the permeable soils and bedrock promoted deep percolation and groundwater-dominated streamflow, despite occurring in a humid, tropical climate. Similarly large baseflow contributions have been found for alpine volcanic catchments in Northern California (Davisson and Rose, 1997; Rose et al., 1996). Overall, these findings point to the need to move beyond the assumption that mountain bedrock is impermeable and demonstrate the usefulness of hydrograph separation for understanding the contributions of interbasin flow and groundwater to streamflow in data-limited catchments.

4.2. Precipitation

The small contribution of precipitation water suggests that the permeable soil and bedrock promotes infiltration rather than surface runoff contributions during storm events in the Diguillí. This finding is common in hydrograph separation studies, where pre-existing water tends to dominate streamflow peaks during storm events (Buttle, 1994), and it is especially common in hydrograph separations performed in permeable catchments (Muñoz-Villers and McDonnell, 2012). An exception to this, however, are snowmelt-dominated and glaciated catchments, which tend to exhibit larger precipitation volumes contributing to streamflow in the form of snow or glacier melt (Cable et al., 2011; Rodriguez et al., 2014; Dahlke et al., 2014). Thus, it appears from our results that the permeable geology of the Diguillín promotes snowmelt recharge rather than direct input of snowmelt to streamflow, despite a major amount of precipitation falling as snow in the uplands.

Chile experiences large inter-annual swings in precipitation, largely in response to El Nino Southern Oscillation (ENSO), with El Niño periods associated with wet anomalies and La Niña periods associated with droughts (Grimm et al., 2000). This study took place during a drier than average water year amidst a decade long drought in central Chile (Reportes Hidrometeorol, 2018). Thus, without multiple years of data, ideally spanning wet and dry years, it is difficult to draw a robust conceptual model from the results of this study, particularly for the precipitation source fraction. Dahlke et al. (2014) found the event water fraction in their glaciated alpine catchment doubled between two study years, which they attributed to the timing of high magnitude precipitation events and soil moisture status of the catchment – two mechanisms that would increase in a wetter year. However, Muñoz-Villers and McDonnell (2012) demonstrated in a tropical montane cloud forest with frequent storm events that permeable soils and bedrock produce minimal event contributions to streamflow. Our results show that event water contributes the least to Diguillín runoff (Fig. 8), due to permeable soils and bedrock (Muñoz-Villers and McDonnell, 2012), a drier than average year, or some combination of the two. Thus, a major question regarding dominant runoff-generation processes in the Diguillín is what rain event, snowmelt, or soil moisture threshold is required for rapid event water delivery to streams, and whether this

threshold is reached in wetter years.

4.3. Possible explanations for the third endmember

The unknown source of water contributes roughly 40% of streamflow in the Diguillín during the winter season (Fig. 9), a sizable volume given that the majority of precipitation and streamflow discharge occurs during this season (Fig. 1). We inferred the tracer values for this endmember from the available streamflow chemistry observations, using our Bayesian model, which for δD and Si were − 55 ± 12‰ and 6.1 ± 2.8 mg/l, respectively. The inferred deuterium isotopic signature reflects a level of enrichment greater than average values for groundwater and precipitation water in this study area, which could conceivably occur in the thick unsaturated zone that exists along reaches of the Diguillín. This enrichment could either be from enriched rainfall infiltrating or from evaporation in the soil or riparian zone. Given that these hillslopes received snow in the winter, and that even the rainfall signature was depleted in the winter months (Fig. 5), it is unlikely that enriched precipitation is the cause for the isotopic values of our estimated third endmember. Alternatively, the Mediterranean climate of the Diguillín could promote soil evaporation and enrichment throughout the hot, dry summers, and the winter precipitation could act to flush this enriched water to the stream.

The inferred Si signature from our Bayesian model (6.1 mg/l) further evidences this flushing theory, since it exhibits an intermediate value between the high-Si groundwater (24.4 mg/l) source and low-Si precipitation (0.2 mg/l) source. Si concentration in water is generally a product of the weathering and dissolution of silicates, which are abundant in terrestrial systems, and thus has been used to infer residence time (Benettin et al., 2015; Frisbee et al., 2012). Some studies have shown Si to be non-conservative (Kirchner, 2003; Christophersen and Hooper, 1992), where kinetic reactions result in Si values to be lower in longer residence time groundwater. Indeed, such kinetic reactions could be found for most 'conservative' tracers, given the appropriate settings. However, recent studies have found Si behavior to be dominated by dissolution and thus a dependable metric for residence time (Benettin et al., 2015; Maher, 2011; Maher, 2010). However, as an added check, we performed the same hierarchical Bayesian mixing model (Eq. (2)) using Cl instead of Si values, and found no significant difference in model estimated proportions between the two tracers. That being said, more data is necessary, and particularly a full analysis of groundwater chemistry evolution should be conducted to determine the most appropriate conservative tracer for this system. Barring any reactivity, the model inferred intermediate Si values suggest that the third endmember comes into contact with Si-bearing rock, such as with interflow or lateral subsurface flow (Newman et al., 1998; Weiler and McDonnell, 2003).

The typical conceptual model of interflow was developed in mesic, forested catchments (Barthold and Woods, 2015; Burns, 2002), where frequent storm events maintain moisture levels in the unsaturated zone throughout extended periods of time or intense storm events produce lateral flow within an event. Studies have found that, while Mediterranean climates are technically semi-arid, the wet season concentrates precipitation and elevates soil moisture enough to generate significant lateral flow volumes (Ohara et al., 2011). Liu et al. (2008) found similar behavior in a semi-arid alpine volcanic catchment, where snowmelt infiltrates the "rubble" land, and flows laterally along the soil-bedrock interface. This flowpath comprised nearly all runoff-generation in their first order catchments, with hardly any event runoff and groundwater contributions (Liu et al., 2008). The geomorphologic requirements for interflow– steep hillslopes of permeable soil, alluvium, or saprolite atop a relatively impermeable bedrock (Weiler and McDonnell, 2003)– exists in the Alto Diguillín subwatershed (Fig. 2). Thus, it is plausible that interflow could substantially contribute to streamflow in the Diguillín in the Alto Diguillín subwatershed.

While this source fits conceptually for the unknown third

endmember, a major source of uncertainty in this study is that we were not able to directly observe or sample any interflow during the wet winter months. However, we were able to sample springs emanating from hillslopes in the Alto Diguillín subwatershed during late summer/early Fall (March). The average and standard deviation of these small springs are 66.2 ± 6.3‰ and 10.2 ± 4.2 mg/l, for δD and Si respectively. These low-volume springs are roughly within one standard deviation of the model-estimated tracer values for the interflow component. Individual springs closer to the streamflow sampling location (e.g. Diguillín outlet), for which we performed the hydrograph separation, have values much closer to the posterior estimated tracer concentrations. Given that these springs were sampled in late summer, these results confirm the existence of enriched water emanating along hillslopes in the Alto Diguillín and add strength to the theory that interflow flushes enriched water to the stream in winter.

If flushing of enriched soil water during winter storms is catchment-scale mechanism for explaining the third unknown endmember, it is worth exploring the finer-scale hillslope processes that may be occurring in the riparian or soil zone. For example, it is possible that a perched saturated zone transmits water rapidly along the soil-bedrock interface (McGlynn and McDonnell, 2003), but relatively high canopy interception (Brodersen et al., 2000) and ET rates in riparian zones (Lupon et al., 2018) promote evaporative enrichment of isotopes. Alternatively, studies have found differing flowpaths within the unsaturated zone based on soil heterogeneity, such as preferential flow through an organic layer imparting significantly different chemical signature on water than the overall unsaturated flow in a hillslope (Hooper et al., 1990). While most of the low-lying agricultural area in the Bío Bio Region has been classified and characterized by the Chilean soil survey, this soil map does not extend to the mountainous areas of the Diguillín watershed. This information would be extremely useful for understanding the mineral composition, thickness, water holding capacity, and moisture retention behavior of the soils throughout the Diguillín. Ultimately, the paucity of observations of hillslope-scale hydrology and soil properties limits our ability to unequivocally identify the third endmember contributing to streamflow in the Diguillín. Given our findings that this source may generate upwards of 40% of winter streamflow (Fig. 9), future work should address this potential runoff-generation mechanism in the Alto Diguillín.

4.4. Implications for regional hydrology and water resources

Understanding how catchments store and transmit water, both on the surface and in the subsurface, is key for water resource management, especially in ungauged or minimally-gauged regions (Sivapalan, 2003). The results of this work have clear management implications for the Diguillín, particularly with respect to climate change adaptation. While our results suggest that streamflow in the Diguillín is not fed directly by snowmelt, it is clear that snowmelt is an important source of recharge to the groundwater system and to streamflow via interflow. Climate change will impact the timing of recharge and snowmelt events, by transitioning precipitation towards rain and triggering snowmelt events earlier. This phase change and timing change will likely impact the overall hydrograph by shifting the centroid of flow earlier (Hidalgo et al., 2009; Stewart et al., 2005) and slowing the melt rates (Musselman et al., 2017). Further, increased ET and shorter periods of near-zero ET due to climate change will result in depleted vadose zone moisture, essentially cutting off the required antecedent wetness for interflow. In some cases this will be offset by an increased frequency of extreme precipitation events, however the direction and magnitude of projected precipitation behavior is still highly uncertain at the regional scale. Groundwater dynamics and mountain front recharge will also shift in response to these changes, and modeling studies suggest that groundwater storage and baseflow volumes will decrease nonlinearly with warming (Markovich et al., 2016). Given that the Diguillín streamflow is comprised of around 75% of groundwater in the dry summers, these decreases in baseflow due to

climate change would impact water availability for irrigation and domestic use in rain-free periods. Hence, more work and particularly numerical modeling is needed in the Diguillín watershed to improve the conceptual model of flowpath and runoff-generation processes and to project the impacts of climate and land use change.

5. Conclusions

Mountain watersheds are not just the headwaters to downstream water supply, they also act as "water towers" storing and releasing snowpack and groundwater downstream each year (Zhang et al., 2018). Understanding how alpine systems store and transmit water is key for managing this resource amidst development and climate change. However, the general lack of groundwater monitoring data in mountain systems poses a "grand challenge" to progress (Sivapalan, 2003). This study posed the question of how much information we can extract from hydrograph separation in a remote, mesoscale, and poorly gauged alpine catchment in Chile. Specifically, our goals were to determine the dominant sources of flow to the Diguillín River overall and characterize their seasonal variation for the water year 2016–17. We applied principal components analysis in order to identify the dominant sources of flow to the Diguillín River in Chile (Fig. 6) and then quantified the source contributions based on spatial and temporal variability in endmember concentration using a hierarchical Bayesian mixing model (Eq. (2)).

The hydrograph separation revealed that, on average, groundwater is the largest and precipitation (e.g. rain and snow) the smallest contributors to streamflow (Fig. 8), while a third endmember, identified in the PCA-analysis, contributes around 40% of the streamflow during the winter wet season (Fig. 9). We hypothesize that interflow is occurring as the third endmember in the Alto Diguillín subwatershed, based on the model-inferred tracer values and the observed presence of alluvium atop impermeable bedrock along certain reaches. More work is necessary to observe and sample these flowpaths, which was not possible during this study due to inaccessibility of sampling sites. The results of this work have implications for water resource management, since groundwater sustains the majority of streamflow in the Diguillín, and development and climate change threaten the quality and quantity of springflow, respectively. Overall, we demonstrate the utility of combining PCA with Bayesian statistical modeling and inference to extract maximum information from a limited field dataset in a remote alpine catchment. The findings of this work alone can guide future water management in the Diguillín, but also provide clear questions for future research.

Declaration of Competing Interest

None.

Appendix

Table 1
Isotope and chemistry data

Sample ID	Season	Type	d2H (permil)	d18O (permil)	pH	EC (uS/cm)	Temp (deg C)	Na (mg/l)	Mg (mg/l)	Si (mg/l)	Cl (mg/l)	K (mg/l)	Ca (mg/l)	Sr (mg/l)
AB1-1	Summer	Cold spring	−70.81	−10.22	6.76	120	12.6	16.46	4.07	22.42	10.14	3.35	10.08	0.06
AB1-2	Fall	Cold spring	−70.31	−10.45	7.23	130	12	16.27	4.13	21.47	10.76	3.38	10.36	0.06
AB3-1	Fall	Cold spring	−71.88	−10.52	6.58	140	11.8	15.53	3.93	19.97	10.63	3.21	9.68	0.05
RE-1	Winter	Cold spring	−70.75	−10.58	7.07	189	11.9	19.22	4.04	20.37	11.73	3.69	10.15	0.06
DH-1	Summer	Hot spring	−85.55	−12.14	7.53	400	43	116.62	4.07	63.26	29.55	8.93	19.5	0.03
DH-2	Summer	Hot spring	−84.66	−12	8.05	510	36.20	100.22	3.72	56.15	25.11	7.75	17.24	0.03
EC1-1	Winter	Hot spring	−81.09	−11.48	7.83	813	28.2	122.06	6.64	44.92	52.63	8.88	29.34	0.08
EC1-2	Spring	Hot spring	−79.41	−10.9	8.72	580	34.70	119.29	5.41	50.35	56.76	8.75	23.72	.07
EC2-1	Winter	Hot spring	−79.11	−10.79	8.53	1267	44.7	214.73	3.07	49.06	125.92	14.05	27.28	0.09
EC2-2	Spring	Hot spring	−78.72	−10.58	8.59	1330	42.2	196.24	2.49	63.95	126.08	14.03	21.43	0.08
EC2-3	Summer	Hot spring	−78.39	−10.42	8.55	1180	48	215.93	2.66	61.61	137.6	15.12	23.65	0.08
EC3-1	Summer	Hot spring	−80.25	−10.67	9.1	600	41.2	161.65	1.56	62.01	28.4	9.41	33.44	0.09
R-12	Spring	Rain	−39.71	−6.92	NA	NA	NA	0.61	0.11	0.15	1.44	0.36	0.55	0.00
R-13	Spring	Rain	−48.02	−7.36	NA	NA	NA	0.55	0.09	0.07	0.58	0.36	0.39	0.00
R-15	Summer	Rain	−22.44	−5.15	NA	NA	NA	1.49	0.19	0.01	2.84	0.1	0.15	0.00
R-16	Summer	Rain	−27.26	−5.98	NA	NA	NA	1.12	0.14	0.05	1.96	0.12	0.24	0.00
R-10	Winter	Rain	−86.7	−12.35	NA	NA	NA	0.07	0.01	0.01	0.1	0.05	1.12	0
R-2	Winter	Rain	−62.39	−9.43	NA	NA	NA	0.44	0.14	0.01	0.62	0.26	0.79	0
R-3	Winter	Rain	−61.58	−9.62	NA	NA	NA	0.39	0.09	0.02	0.68	0.15	1.55	0
R-6	Winter	Rain	−83.35	−11.6	NA	NA	NA	0.27	0.05	0.01	0.44	0.06	0.29	0
R-7	Winter	Rain	−78.71	−11.22	NA	NA	NA	0.25	0.03	0.01	0.42	0.05	0.92	0
R-9	Winter	Rain	−81.88	−11.79	NA	NA	NA	0.08	0.03	0.01	0.04	0.08	0.21	0
GDD-2	Winter	Snow	−76.68	−11.13	NA	NA	NA	0.08	0.01	0	0.08	0.06	0.05	0
GDD-4	Winter	Snow	−73.01	−10.86	NA	NA	NA	0.18	0.02	0.01	0.18	0.19	0.1	0
GDD-5	Winter	Snow	−74.03	−11.08	NA	NA	NA	0.11	0	0.02	0.2	0.1	0.03	0
SRL-1	Winter	Snow	−80.81	−11.85	NA	NA	NA	0.28	0.02	0.01	0.43	0.09	0.06	0
SRL-3	Winter	Snow	−76.21	−11.6	NA	NA	NA	0.2	0.02	0	0.35	0.08	0.07	0
VAC-3	Winter	Snow	−79.94	−11.51	NA	NA	NA	0.3	0.04	0.07	0.52	0.31	0.23	0
VAC-4	Winter	Snow	−85.55	−12.54	NA	NA	NA	0.12	0.01	0.02	0.23	0.12	0.05	0
VAC-5	Winter	Snow	−75.81	−11.6	NA	NA	NA	0.14	0.01	0.02	0.19	0.11	0.05	0
DB-1	Winter	Streamflow	−66.92	0.23	7.98	167	8.69	19.8	2.8	16.85	9.85	2.63	9.05	0.04
DB-11	Spring	Streamflow	−64.93	−9.31	7.87	50	10	8.81	1.38	10.48	3.87	1.13	5.28	0.02
DB-12	Spring	Streamflow	−64.46	−9.59	8.1	100	13.8	10.82	1.69	11.97	5.71	1.6	6.53	0.03
DB-13	Spring	Streamflow	−66.12	−9.75	7.3	153	14.5	16.37	2.25	16.07	10.53	3.93	8.19	0.04
DB-13.5	Spring	Streamflow	−65.64	−9.4	NA	NA	NA	20.38	2.8	19.26	11.41	3.14	9.77	0.05
DB-14	Summer	Streamflow	−63.9	−8.85	7.64	198	17.5	18.99	2.67	17.60	10.23	2.58	8.85	0.04
DB-15	Summer	Streamflow	−66.72	−9.59	7.86	170	14.8	19.76	2.7	17.71	12.85	4.7	9.57	0.05
DB-16	Summer	Streamflow	−67.06	−9.77	8.18	190	16.2	22.04	3.11	19.68	12.27	3.04	10.39	0.05
DB-17	Summer	Streamflow	−66.84	−9.80	7.47	150	15	22.73	3.2	19.22	12.6	3.13	9.94	0.05
DB-18	Summer	Streamflow	−67.31	−9.78	7.2	140	10	19.81	2.98	17.59	11.32	2.78	9.69	0.05
DB-19	Fall	Streamflow	−67.38	−9.85	8.59	210	13.5	27.26	2.84	19.44	14.76	2.91	10.51	0.05
DB-2	Winter	Streamflow	−68.91	−10	8.07	170	8.19	19.07	2.67	17.17	9.84	2.68	9.43	0.04
DB-20	Fall	Streamflow	−68.65	−9.83	8.68	160	16.10	22.55	3.21	19.38	13.06	2.97	10.56	0.05
DB-21	Fall	Streamflow	−68.72	−10.02	8.32	180	15	22.75	3.21	19.38	13.01	2.98	10.5	0.05
DB-22	Fall	Streamflow	−70.59	−10.21	8.13	170	11.7	23.47	3.28	19.51	13	2.96	10.88	0.05
DB-3	Winter	Streamflow	−64.57	−9.65	7.13	84	6.5	8.49	1.32	9.71	4.35	1.23	5.09	0.02
DB-4	Winter	Streamflow	−64.88	−9.67	7.48	67	8.1	6.9	0.96	7.69	3.21	0.94	4.21	0.02
DB-5	Winter	Streamflow	−66.94	−9.69	7.35	76	9.1	7.65	1.12	8.6	4.36	1.09	5.01	0.02
DB-6	Winter	Streamflow	−66.31	−9.75	7.56	101	7.9	9.58	1.45	10.46	4.73	1.42	6.2	0.03
DB-7	Winter	Streamflow	−66.62	−9.82	7.57	114	9.5	12.19	1.72	11.92	6.6	2.18	6.8	0.03
DB-8	Winter	Streamflow	−62.95	−9.30	7.29	79	9.30	9.1	1.46	10.37	6.44	2.99	5.63	0.03
DB-9	Winter	Streamflow	−61.31	−8.91	7.57	79	10.7	9.80	1.57	13.05	8	4.62	5.96	0.03
R-4	Winter	Chillan Rain	−38.9	−6.58	NA	NA	NA	0.27	0.05	0.03	0.4	0.07	1.7	0
R-5	Winter	Chillan Rain	−40.03	−6.47	NA	NA	NA	0.63	0.09	0	1.05	0.05	3.16	0
R-8	Winter	Chillan Rain	−85.4	−11.73	NA	NA	NA	0.06	0.02	0.02	0.07	0.02	1.7	0
Vt-1	Winter	Warm Spring	−73.99	−10.74	6.28	297	15.1	33.94	6.6	27.78	20.52	5.98	14.65	0.07
Vt-2	Spring	Warm Spring	−74.95	−10.79	6.27	314	15	32.68	6.33	26.09	20.36	6.05	15.66	0.07
Vt-3	Summer	Warm Spring	−75.44	−10.78	6.31	280	15.7	33.51	6.96	28.08	22.82	6.1	15.56	0.08
Vt-4	Fall	Warm Spring	−74.91	−10.6	6.12	310	15.9	34.68	6.78	29.05	22.29	6.27	15.32	0.08

References

Andermann, C., Longuevergne, L., Bonnet, S., Crave, A., Davy, P., Gloaguen, R., 2012. Impact of transient groundwater storage on the discharge of Himalayan rivers. Nat. Geosci. 5 (2), 127–132. https://doi.org/10.1038/ngeo1356.

Arce, A., 2014. Evaluating a fractured media groundwater system using a hydrologic model (Master's thesis). Universidad de Concepcion, Chillan, Chile.

Arendt, C., Aciego, S., Hetland, E., 2015. An open soure Bayesian Monte Carlo isotope mixing model with applications in Earth surface processes. Geochem. Geophys. Geosyst. 16, 1274–1292. https://doi.org/10.1002/2014GC005683.

Arumí, J.L., Maureira, H., Souvignet, M., Rivera, D., Oyarzun, R., 2012. Where does the water go? Understanding geohydrological behavior of Andean catchments in South-Central Chile. Hydrol. Sci. J. 40. https://doi.org/10.1080/02626667.2014.934250.

Barnett, T.P., Adam, J.C., Lettenmaier, D.P., 2005. Potential impacts of a warming climate on water availability in snow-dominated regions. Nature 438 (November), 303–309. https://doi.org/10.1038/nature04141.

Barthold, F.K., Woods, R.A., 2015. Stormflow generation: A meta analysis of field

evidence from small, forested catchments. Water Resour. Res. 51 (5), 3730–3753. https://doi.org/10.1002/2014WR016221. arXiv: 2014WR016527 [10.1002].

Bearup, L.A., Maxwell, R.M., Clow, D., McCray, J., 2014. Hydrological effects of forest transpiration loss in bark beetle-impacted watersheds. Nature Climate Change 4 (6), 481–486. https://doi.org/10.1038/NCLIMATE2198.

Benettin, P., Bailey, S., Campbell, J., Green, M., Rinaldo, A., Likens, G., Botter, G., 2015. Linking water age and solute dynamics in streamflow at the Hubbard Brook Experimental Forest, NH, USA. Water Resour. Res. 9256–9272. https://doi.org/10.1002/2013WR014222.

Beniston, M., Diaz, H.F., Bradley, R.S., 1997. Climatic change at high elevation sites: an overview. Climatic Change 36, 233–251. https://doi.org/10.3406/rga.2005.2342.

Brodersen, C., Pohl, S., Lindenlaub, M., Leibundgut, C., Wilpert, K.V., 2000. Influence of vegetation structure on isotope content of throughfall and soil water. Hydrol. Process. 14 (8), 1439–1448. https://doi.org/10.1002/1099-1085(20000615)14:8<1439::AID-HYP985>3.0.CO;2-3.

Burns, D., 2002. Stormflow-hydrograph separation based on isotopes: the thrill is gone- what's next? Hydrol. Process. 16 (7), 1515–1517. https://doi.org/10.1002/hyp.5008.

Buttle, J., 1994. Isotope hydrograph separations and rapid delivery of pre event water from drainage basins. Prog. Phys. Geogr. 18 (1), 16–41. https://doi.org/10.1177/030913339401800102.

Cable, J., Ogle, K., Williams, D., 2011. Contribution of glacier meltwater to streamflow in the Wind River Range, Wyoming, inferred via a Bayesian mixing model applied to isotopic measurements. Hydrol. Process. 25 (14), 2228–2236. https://doi.org/10.1002/hyp.7982.

Christophersen, N., Hooper, R.P., 1992. Multivariate analysis of stream water chemical data: The use of principal components analysis for the endmember mixing problem. Water Resour. Res. 28 (1), 99–107. https://doi.org/10.1029/91WR02518.

Cristea, N.C., Lundquist, J.D., Loheide, S.P., Lowry, C.S., Moore, C.E., 2014. Modelling how vegetation cover affects climate change impacts on streamflow timing and magnitude in the snowmelt-dominated upper Tuolumne Basin, Sierra Nevada. Hydrological Processes 28 (12), 3896–3918. https://doi.org/10.1002/hyp.9909.

Dahlke, H.E., Lyon, S.W., Jansson, P., Karlin, T., Rosqvist, G., 2014. Isotopic investigation of runoff generation in a glacierized catchment in northern Sweden. Hydrol. Process. 28 (3), 1383–1398. https://doi.org/10.1002/hyp.9668.

Davisson, M., Rose, T., 1997. Comparative Isotope Hydrology Study of Groundwater Sources and Transport in the Three Cascade Volcanoes of Northern California. Lawrence Livermore National Laboratory.

Dixon, H.J., Murphy, M.D., Sparks, S.J., Chávez, R., Dunkley, P.N., Young, S.R., Pringle, M.R., 1999. The geology of Nevados de Chillan volcano, Chile. Revista geologica de Chile, 1–29.

Ficklin, D., Stewart, I.T., Maurer, E.P., 2013. Climate change impacts on streamflow and subbasin-scale hydrology in the Upper Colorado River Basin. PloS one 8 (8), e71297. https://doi.org/10.1371/journal.pone.0071297.

Fischer, B.M., van Meerveld, H., Seibert, J., 2017. Spatial variability in the isotopic composition of rainfall in a small headwater catchment and its effect on hydrograph separation. J. Hydrol. 547, 755–769. https://doi.org/10.1016/j.jhydrol.2017.01.045.

Frisbee, M.D., Phillips, F.M., Campbell, A.R., Liu, F., Sanchez, S.a., 2011. Streamflow generation in a large, alpine watershed in the southern Rocky Mountains of Colorado: Is streamflow generation simply the aggregation of hillslope runoff responses? Water Resour. Res. 47 (6), W06512. https://doi.org/10.1029/2010WR009391.

Frisbee, M.D., Phillips, F.M., Weissmann, G.S., Brooks, P.D., Wilson, J.L., Campbell, A.R., Liu, F., 2012. Unraveling the mysteries of the large watershed black box: implications for the streamflow response to climate and landscape perturbations. Geophys. Res. Lett. 39 (1). https://doi.org/10.1029/2011GL050416.

Frisbee, M.D., Tysor, E.H., Stewart-Maddox, N.S., Tsinnajinnie, L.M., Wilson, J.L., Granger, D.E., Newman, B.D., 2016. Is there a geomorphic expression of interbasin groundwater flow in watersheds? interactions between interbasin groundwater flow, springs, streams, and geomorphology. Geophys. Res. Lett. 43 (3), 1158–1165. https://doi.org/10.1002/2015GL067082.

Genereux, D., 1998. Quantifying uncertainty in tracer-based hydrograph separations. Water Resour. Res. 34 (4), 915. https://doi.org/10.1029/98WR00010.

Goulden, M.L., Bales, R.C., 2014. Mountain runoff vulnerability to increased evapo- transpiration with vegetation expansion. PNAS 111 (39), 14071–14075. https://doi.org/10.1073/pnas.1319316111.

Grimm, A.M., Barros, V.R., Doyle, M.E., 2000. Climate variability in southern South America associated with El Niño and La Niña events. J. Clim. 13 (1), 35–58. https://doi.org/10.1175/1520-0442(2000) 013<0035:CVISSA>2.0.CO;2.

Hidalgo, H.G., Das, T., Dettinger, M.D., Cayan, D.R., Pierce, D.W., Barnett, T.P., Nozawa, T., 2009. Detection and attribution of streamflow timing changes to climate change in the Western United States. J. Clim. 22 (13), 3838–3855. https://doi.org/10.1175/2009JCLI2470.1.

Hoffman, M.D., Gelman, A., 2014. The no-u-turn sampler: adaptively setting path lengths in hamiltonian monte carlo. J. Mach. Learn. Res. 15 (1), 1593–1623.

Hooper, R.P., 2003. Diagnostic tools for mixing models of stream water chemistry. Water Resour. Res. 39 (3), 1–13. https://doi.org/10.1029/2002WR001528.

Hooper, R.P., Christophersen, N., Peters, N.E., 1990. Modelling streamwater chemistry as a mixture of soilwater end-members - An application to the Panola Mountain catchment, Georgia, U.S.A. J. Hydrol. 116 (1–4), 321–343. https://doi.org/10.1016/0022-1694(90)90131-G.

Kassambara, A., Mundt, F., 2017. Factoextra: extract and visualize the results of multi- variate data analyses. R package version 1.0.5. Retrieved from https://CRAN.R-project.org/package=factoextra.

Kirchner, J.W., 2003. A double paradox in catchment hydrology and geochemistry. Hydrol. Process. 17 (4), 871–874. https://doi.org/10.1002/hyp.5108.

Klaus, J., McDonnell, J.J., 2013. Hydrograph separation using stable isotopes: review and evaluation. J. Hydrol. 505, 47–64. https://doi.org/10.1016/j.jhydrol.2013.09.006.

Knowles, N., Dettinger, M.D., Cayan, D.R., 2006. Trends in snowfall versus rainfall in the western United States. J. Clim. 19 (18), 4545–4559. https://doi.org/10.1175/JCLI3850.1.

Liu, F., Bales, R.C., Conklin, M.H., Conrad, M.E., 2008. Streamflow generation from snowmelt in semi-arid, seasonally snow-covered, forested catchments, Valles Caldera, New Mexico. Water Resour. Res. 44 (12), 1–13. https://doi.org/10.1029/2007WR006728.

Lupon, A., Ledesma, J.L.J., Bernal, S., 2018. Riparian evapotranspiration is essential to simulate streamflow dynamics and water budgets in a mediterranean catchment. Hydrol. Earth Syst. Sci. 22 (7), 4033–4045. https://doi.org/10.5194/hess-22-4033-2018.

Maher, K., 2010. The dependence of chemical weathering rates on fluid residence time. Earth Planet. Sci. Lett. 294 (1), 101–110. https://doi.org/10.1016/j.epsl.2010.03.010.

Maher, K., 2011. The role of fluid residence time and topographic scales in determining chemical fluxes from landscapes. Earth Planet. Sci. Lett. 312 (1–2), 48–58. https://doi.org/10.1016/j. epsl.2011.09.040.

Mailloux, J., Ogle, K., Frost, C., 2014. Application of a Bayesian model to infer the contribution of coalbed natural gas produced water to the Powder River, Wyoming and Montana. Hydrol. Process. 28, 2361–2381. https://doi.org/10.1002/hyp.9784.

Mankin, J.S., Williams, A.P., Seager, R., Smerdon, J.E., Horton, R.M., 2018. Blue water trade-offs with vegetation in a CO2-enriched climate. Geophys. Res. Lett. 45, 3115–3125. https://doi.org/10.1002/2018GL077051.

Markovich, K.H., Maxwell, R.M., Fogg, G.E., 2016. Hydrogeological response to climate change in alpine hillslopes. Hydrol. Process. https://doi.org/10.1002/hyp.10851.

McDonnell, J.J., Bonell, M., Stewart, M.K., Pearce, J.A., 1990. Deuterium variations in storm rainfall: implications for stream hydrograph separation. Water Resour. Res. 26 (3), 455–458.

McGlynn, B.L., McDonnell, J.J., 2003. Quantifying the relative contributions of riparian and hillslope zones to catchment runoff. Water Resour. Res. 39 (11). https://doi.org/10.1029/2003WR002091.

Mcintosh, J., McDonnell, J.J., Peters, N.E., 1999. Tracer and hydrometric study of pre- ferential flow in large undisturbed soil cores from the Georgia Piedmont, USA. Hydrol. Process. 13, 139–155. https://doi.org/10.1002/(SICI)1099-1085(19990215)13:2<139::AID-HYP703>3.0.CO;2-E.

Muñoz-Villers, L.E., McDonnell, J.J., 2012. Runoff generation in a steep, tropical montane cloud forest catchment on permeable volcanic substrate. Water Resour. Res. 48 (9). https://doi.org/10.1029/2011WR011316.

Musselman, K.N., Clark, M.P., Liu, C., Ikeda, K., Rasmussen, R., 2017. Slower snowmelt in a warmer world. Nature Climate Change 7 (3), 214–219. https://doi.org/10.1038/nclimate3225.

Newman, D., Campbell, A.R., Wilcox, P., 1998. Lateral subsurface flow pathways in a semiarid ponderosa pine hillslope. Water Resour. Res. 34 (12), 3485–3496.

Ogle, K., Tucker, C., Cable, J.M., 2014. Beyond simple linear mixing models: Process- based isotope partitioning of ecological processes. Ecol. Appl. 24 (1), 181–195. https://doi.org/10.1890/1051-0761-24.1.181.

Ohara, N., Kavvas, M.L., Easton, D., Dogrul, E.C., Yoon, J.Y., Chen, Z.Q., 2011. Role of snow in runoff processes in a subalpine hillslope: field study in the ward creek wa- tershed, lake tahoe, california, during 2000 and 2001 water years. J. Hydrol. Eng. 16 (6), 521–533. https://doi.org/10.1061/(ASCE)HE.1943-5584.0000348.

Ohlanders, N., Rodriguez, M., McPhee, J., 2013. Stable water isotope variation in a Central Andean watershed dominated by glacier and snowmelt. Hydrol. Earth Syst. Sci. 17 (3), 1035–1050. https://doi.org/10.5194/hess-17-1035-2013.

Reportes Hidrometeorológicas, 2018. Retrieved from http://snia.dga.cl/BNAConsultas/reportes.

Rodriguez, M., Ohlanders, N., McPhee, J., 2014. Estimating glacier and snowmelt con- tributions to stream flow in a Central Andes catchment in Chile using natural tracers. Hydrol. Earth System Sci. Discussions 11 (7), 8949–8994. https://doi.org/10.5194/hessd-11-8949-2014.

Rodriguez, M., Ohlanders, N., Pellicciotti, F., Williams, M.W., Mcphee, J., 2016. Estimating runoff from a glacierized catchment using natural tracers in the semi-arid Andes cordillera. Hydrol. Process. 30, 3609–3626. https://doi.org/10.1002/hyp.10973.

Rose, T., Davisson, M., Criss, R., 1996. Isotope hydrology of voluminous cold springs in fractured rock from an active volcanic region, northeastern California. J. Hydrol. 179, 207–236.

Sanchez-Murillo, R., Aguirre-Duenas, E., Gallardo-Amestica, M., Moya-Vega, P., Birkel, C., Esquival-Hernandez, G., Boll, J., 2018. Isotopic Characterization of Waters Across Chile. In: Andean hydrology. pp. 205–230.

Schmieder, J., Hanzer, F., Marke, T., Garvelmann, J., Warscher, M., Kunstmann, H., Strasser, U., 2016. The importance of spatiotemporal snowmelt variability for iso- topic hydrograph separation in a high elevation catchment. Hydrol. Earth System Sci. Discussions 20, 5015–5030. https://doi.org/10.5194/hess-2016-128.

Sivapalan, M., 2003. Prediction in ungauged basins: a grand challenge for theoretical hydrology. Hydrol. Process. 17, 3163–3170. https://doi.org/10.1002/hyp.5155.

Sklash, M.G., Farvolden, R.N., Fritz, P., 1976. A conceptual model of watershed response to rainfall, developed through the use of oxygen-18 as a natural tracer. Can. J. Earth Sci. 13 (5), 715. https://doi.org/10.1139/e76-076.

Stan Development Team, 2018. RStan: the R interface to Stan. R package version 2.17.3. Retrieved from http://mc-stan.org/.

Stewart, I.T., Cayan, D.R., Dettinger, M.D., 2005. Changes toward earlier streamflow timing across Western North America. J. Clim. 18, 1136–1155.

Tague, C., Grant, G.E., 2009. Groundwater dynamics mediate low-flow response to global warming in snow-dominated alpine regions. Water Resour. Res. 45 (7). https://doi.

org/10.1029/2008WR007179.

Taylor, S., Feng, X., Kirchner, J.W., Osterhuber, R., Klaue, B., Renshaw, C.E., 2001. Isotopic evolution of a seasonal snowpack and its melt. Water Resour. Res. 37 (3), 759–769. https://doi.org/10.1029/2000WR900341.

Taylor, S., Feng, X., Williams, M., McNamara, J., 2002. How isotopic fractionation of snowmelt affects hydrograph separation. Hydrol. Process. 16 (18), 3683–3690. https://doi.org/10.1002/hyp. 1232.

Weiler, M., McDonnell, J.J., 2003. Conceptualizing lateral preferential flow and flow networks and simulating the effects on gauged and ungauged hillslopes. Water

Resour. Res. 43 (3). https://doi.org/10.1029/2006WR004867.

Wilson, J.L., Guan, H., 2004. Mountain-block hydrology and mountain-front recharge. In: In: Hogan, J.F., Phillips, F., Scanlon, B.R. (Eds.), Groundwater recharge in a desert environment: the southwestern united states, vol. 9. American Geophysical Union, Washington, DC, pp. 113–137.

Zhang, Q., Knowles, J.F., Barnes, R.T., Cowie, R.M., Rock, N., Williams, M.W., 2018. Surface and subsurface water contributions to streamflow from a mesoscale watershed in complex mountain terrain. Hydrol. Process. 32 (7), 954–967. https://doi. org/10.1002/hyp.11469.